Macromolecules
ARTICLE

Macromolecules **2010**, *43*, 1299–1308 **1299**
DOI: 10.1021/ma902104m

Reinforcing the Hydrophobicity of Polymeric Surfaces from Fluorinated Star Polymers and Nanogels

J. Poly,*,†,‡ E. Ibarboure,† J. Rodriguez-Hernandez,†,§ D. Taton,† and E. Papon†

†*Laboratoire de Chimie des Polymères Organiques, Université de Bordeaux-CNRS-ENSCPB, 16 avenue Pey Berland, 33607 Pessac, France,* ‡*Laboratoire de Chimie Organique, Bioorganique et Macromoléculaire, Université de Haute Alsace-CNRS-ENSCMu, 3 rue Alfred Werner, 68093 Mulhouse, France, and* §*Instituto de Ciencia y Tecnología de Polímeros, CSIC, C/Juan de la Cierva 328006 Madrid, Spain*

Received September 22, 2009; Revised Manuscript Received December 21, 2009

ABSTRACT: Nanogels and starlike "arm-first" polymers based on 1*H*,1*H*,2*H*,2*H*-perfluorodecyl acrylate were designed by controlled radical cross-linking copolymerization in solution, using ethyl 2-[(phenylcarbonothioyl)sulfanyl]propanoate as a reversible chain transfer agent. Investigations into the structure of these fluorinated branched polymers by means of atomic force microscopy (AFM), differential scanning calorimetry, and polarized optical microscopy revealed a crystalline organization which decreased as the cross-link density increased. Films were prepared from these branched architectures by coating on various substrates. Their properties were studied in comparison with films prepared from linear homologues. Contact angle measurements showed similar hydrophobicity after coating. However, a significant decrease of hydrophobicity was observed after annealing in the case of films prepared from linear polymers, whereas it was almost preserved for films corresponding to branched architectures. For films of same thickness, this observation was due to an important dewetting of the substrate in the case of linear polymers whereas this phenomenon was inhibited in the case of branched architectures, as revealed by optical microscopy and AFM analyses.

Introduction

The small size of fluorine combined with its very high electronegativity confers to C−F bonds very specific properties, with in particular high bond energy and very low polarizability. Since the development of polytetrafluoroethylene in the late 1930s,[1] these two characteristics have been built on for the preparation of polymeric materials possessing unique related features such as high mechanical strength, thermal stability, and chemical inertness as well as low friction coefficient and surface energy.[2−4] Of particular interest, these properties result in surfaces exhibiting excellent weatherability and unwettability.[2−4]

However, the very low surface energy of fluoropolymers is also generally responsible for poor adhesion on hydrophilic substrates, which may cause their dewetting. This phenomenon can be prevented either by a "precoating" approach through a preliminary treatment of the substrate favoring its compatibility with the fluorinated film or by a "postcoating" approach consisting of a subsequent curing of the surface.[5] In this work, we propose an alternative way to the second approach using branched soluble macromolecules, namely nanogels and starlike polymers, which allows for the preparation of reinforced fluorinated films through the concomitant ab initio introduction of cross-links.

These fluorinated branched polymers were designed by controlled radical cross-linking copolymerization (CRCC), following the reversible addition−fragmentation chain transfer (RAFT) process. Various fluoro-based polymers have already been achieved by resorting to controlled/living polymerization methods,[6,7] but to the best of our knowledge, we propose here the first synthesis of fluorinated nanogels and core-cross-linked starlike polymers. CRCC is a recently developed synthetic methodology[8] which has been yet applied to design miscellaneous macromolecular topologies and shapes, from globular to starlike architectures.[9,10] The final shape is governed by the cross-links distribution along constitutive (or primary) chains (Figure 1), which can be properly controlled by playing either on the respective reactivities of monomers or on the addition process implemented (for instance, a semicontinuous addition of the comonomers versus a batch process may lead to different structures, all other parameters being kept the same).[11,12]

In previous contributions, two of us applied CRCC to the synthesis of nanogels based on acrylic acid, acrylamide,[13] and vinyl acetate.[14] Nanogels can be defined as soluble highly branched macromolecules having a network structure and dimensions under 100 nm.[15] We also elaborated on a predictive kinetic model of CRCC based on a necessary distinction between intra- and intermolecular cross-linking, leading to a key equation governing the evolution of the branched macromolecules concentration.[12]

In the present work, we applied for the first time CRCC to the synthesis of both fluorinated nanogels and starlike polymers based on 1*H*,1*H*,2*H*,2*H*-perfluorodecyl acrylate (PFDA) as monomer. Therefore, the main chains were decorated with pendant fluorinated side chains. For the nanogels synthesis, 1,4-butanediol diacrylate (BDDA) was used as a cross-linker. The similar reactivities of acrylic functions of PFDA and BDDA ensured a regular distribution of cross-links along primary chains, resulting in an expected globular structure (Figure 2a).[11,12] Concomitantly, linear poly(PFDA) precursors grown by RAFT were cross-linked by divinylbenzene (DVB), leading to starlike polymers through the "arm-first" methodology (Figure 2b).[9,16] In both cases, ethyl 2-[(phenylcarbonothioyl)sulfanyl]propanoate was used as the chain-transfer agent (CTA). Its efficiency in controlling the polymerization of acrylic and styrenic monomers has been already reported.[17]

Investigations into the surface properties of these different branched fluoro-based polymers revealed that benefit can be

*Corresponding author. E-mail: julien.poly@uha.fr.

Published on Web 01/14/2010

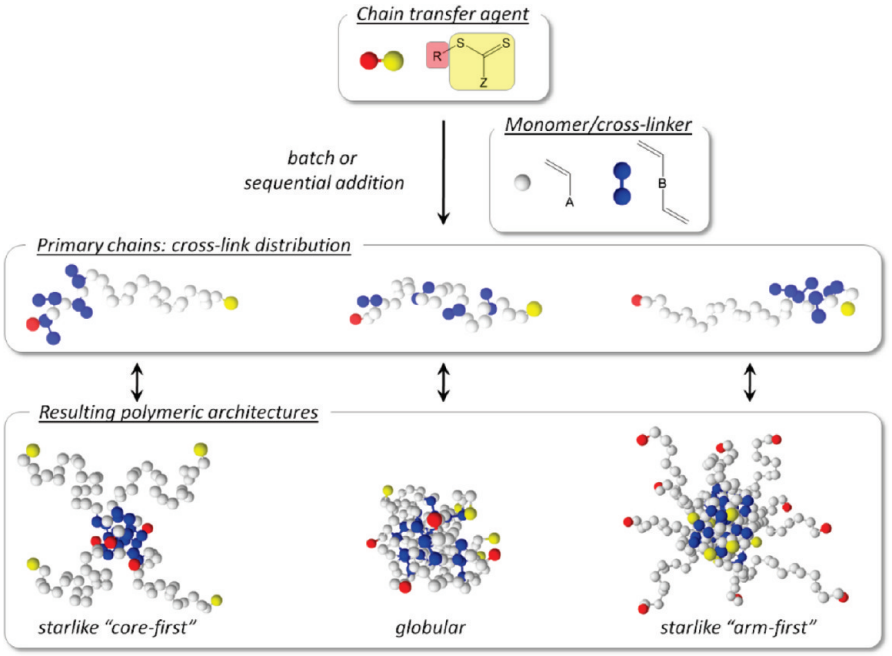

Figure 1. Controlled radical cross-linking (co)polymerization applied to the synthesis of branched macromolecules: the final shape depends on the cross-links distribution along primary chains.[12]

taken from branched architectures to prevent the dewetting of films on substrates and hence to preserve the surface hydrophobicity as opposed to their linear homologues.

Experimental Section

Materials. *S*-(Thiobenzoyl)thioglycolic acid (99%), ethyl 2-mercaptopropionate (≥95%), 1*H*,1*H*,2*H*,2*H*-perfluorodecyl acrylate (PFDA, 97%), 1,4-butanediol diacrylate (BDDA, 90%), divinylbenzene (DVB, 85%), 2,2-azobis(isobutyronitrile) (AIBN, ≥98%), and α,α,α-trifluorotoluene (TFT, ≥99%) were purchased from Sigma-Aldrich. AIBN was recrystallized twice from ethanol prior to use. BDDA was purified by distillation under reduced pressure. All the other reactants were used as received. Ethyl 2-[(phenylcarbonothioyl)sulfanyl]propanoate used as the chain transfer agent (CTA) was synthesized following a procedure described elsewhere.[18]

Polymerization Procedures. All polymerizations were carried out under a nitrogen atmosphere in Schlenk flasks equipped with a magnetic bar.

Synthesis of Linear Polymers and Nanogels. The molar concentration of acrylic functions was kept the same in all experiments: $C_0 = [\text{PFDA}]_0 + 2[\text{BDDA}]_0 = 0.500$ mol/kg. The proportion of initiator was 0.20%C_0. The concentration in CTA was $C_0/50$ or $C_0/100$, depending on the targeted degree of polymerization (DP). In a typical experiment, 1.0 mg of AIBN (6.0×10^{-3} mmol), 15.1 mg of CTA (5.95×10^{-2} mmol), 29.5 mg of BDDA (1.49×10^{-1} mmol), 1.387 g of PFDA (2.68 mmol), and TFT (5.95 g) were added in this order into a flame-dried Schlenk flask. Each solution was thoroughly deoxygenated by three freeze−pump−thaw cycles. The flasks were filled with nitrogen gas and placed in an oil bath maintained at 70 °C for 24 h under magnetic stirring. Solvent was then evaporated under vacuum, and polymers samples were dried under reduced pressure. The ^{1}H NMR spectrum of this sample is shown in Figure 3. The conversion of acrylic functions α can be estimated as follows (residual monomers are not removed):

$$\alpha = 1 - 2/3\frac{I_{r,p,q}}{I_{g,k,s}}$$

where $I_{r,p,q}$ and $I_{g,k,s}$ are integers relative to protons r, p, q and g, k, s, respectively. In the present case, α = 94%. SEC and DSC results for this sample are given in Tables 1 and 2.

Synthesis of a Starlike Polymer. The linear samples with a targeted DP of 100 described above were then used as macromolecular CTAs for a subsequent cross-linking. To this end, 500 mg of this precursor (9.60×10^{-6} mol), 29.0 mg of DVB (2.23×10^{-1} mmol), and 2.0 mL of TFT were added in a Schlenk flask. After three freeze−pump−thaw cycles, the flask was filled with nitrogen gas and placed in an oil bath maintained at 110 °C for 64 h under magnetic stirring. Precipitation of the product at ambient temperature in TFT allowed for an easy separation of stars from residual monomers and a fraction of linear precursors through successive removals of supernatant and redissolving of the product in TFT at 40 °C (DVB, PFDA, and linear poly(PFDA) are soluble in TFT at ambient temperature). The ^{1}H NMR spectrum of this sample is shown in Figure 5. The average number of DVB units (y) per arm (z) can be estimated. Let I and I' be the integers of signals comprised between 4.45 and 4.85 ppm and 7.40 and 7.70 ppm, respectively. I corresponds to $192z$ protons (two protons per repeating unit and experimental DP of linear precursors, determined by ^{1}H NMR spectroscopy, equal to 96). I' corresponds to $4y + 5z$ aromatic protons (four protons per DVB unit and five per dithioester terminal function). Hence

$$\frac{y}{z} = \frac{192I' - 5I}{4I}$$

In the present case, $y/z = 3.0$ DVB unit per chain on average. SEC and DSC results for this sample are given in Tables 1 and 2.

Characterizations. Compositions and conversions were determined by means of ^{1}H NMR spectroscopy in deuterated trifluoroacetic acid on a Bruker AC-400 spectrometer.

Differential scanning calorimetry (DSC) studies were performed on a DSC Q100 TA Instruments. Enthalpy constant and temperature constant calibrations were performed using indium (1.75 mg) as a standard metal which was heated above its melting transition from 100 to 180 °C with a rate of 10 °C/min. The cell constant is obtained by comparison of the measured heat of fusion (28.06 J/g) to the tabulated value (28.71 J/g). The temperature calibration is obtained by comparison of the measured melting point (157.95 °C) to the tabulated value (156.60 °C). For the samples, the temperature range was 0−100 °C. The heating and cooling rates were 10 °C/min. The

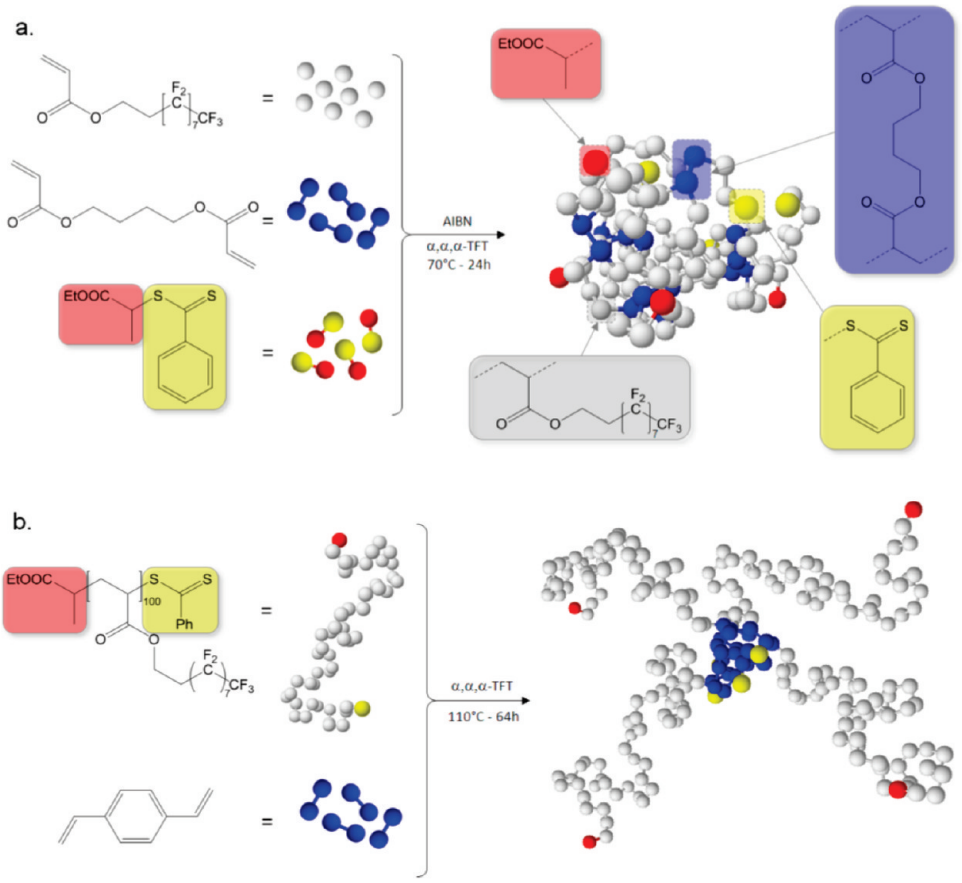

Figure 2. Controlled radical cross-linking polymerization (CRCC) implemented to the synthesis of fluorinated nanogels (a) and starlike polymers (b).

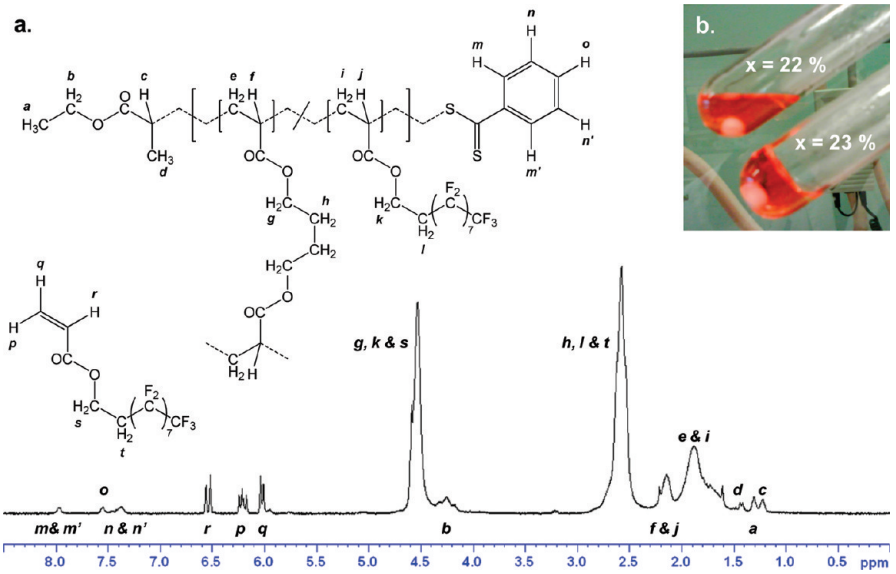

Figure 3. (a) Typical ^{1}H NMR spectrum of a poly(1*H*,1*H*,2*H*,2*H*-perfluorodecyl acrylate)-based nanogel in CF_3-COOD. Total initial concentration of acrylic functions: $C_0 = 0.500$ mol/kg. Initial concentration of chain transfer agent: $[CTA]_0 = 1.00 \times 10^{-2}$ mol/kg. Initial proportion of acrylic functions belonging to cross-linker molecules: $x = 10.0\%$. (b) Transition between soluble ($C_0 = 0.500$ mol/kg; $[CTA]_0 = 1.00 \times 10^{-2}$ mol/kg; $x = 22.0\%$) and insoluble product (macroscopic gel; $C_0 = 0.500$ mol/kg; $[CTA]_0 = 1.00 \times 10^{-2}$ mol/kg; $x = 23.0\%$) at complete conversions.

melting temperatures were measured during the second heating run, at the onset point of the heat flow curve, defined as the point of intersection of the extrapolated baseline with the extrapolated tangent drawn at the point of greatest slope on the leading edge of the peak. Transition massic enthalpies were determined by integration of the peak.

The anisotropy of the products was observed by the use of an optical microscope (Zeiss Axioskop 40) under polarized light and equipped with a numeric camera coupled to a computer, enabling to record the images of each crystallization event. The preliminary preparation of the samples consisted of depositing a few milligrams of the product over a microscope glass slide and heating

Table 1. Steric Exclusion Chromatography Experiments Results for Poly(1*H*,1*H*,2*H*,2*H*-perfluorodecyl acrylate)-Based Polymers in Hexafluoroisopropanol[a]

sample type	DP of primary chains	x (%)	M_n (g/mol)	M_w (g/mol)	M_w/M_n
linear	50	0	8.37×10^3	1.05×10^4	1.25
nanogel	50	10.0	1.32×10^4	2.16×10^4	1.64
nanogel	50	15.0	1.92×10^4	4.16×10^4	2.17
nanogel	50	20.0	2.16×10^4	1.04×10^5	4.83
nanogel	50	22.0		over high limit	
linear	100	0	1.53×10^4	1.90×10^4	1.24
starlike	100	3.0 cross-links per chain	2.69×10^4	4.53×10^4	1.69

[a] DP: degree of polymerization. x: initial proportion of acrylic functions belonging to cross-linker molecules. Apparent number average molar masses (M_n), mass average molar masses (M_w), and polydispersity indexes (M_w/M_n), relative to poly(methyl methacrylate) standards.

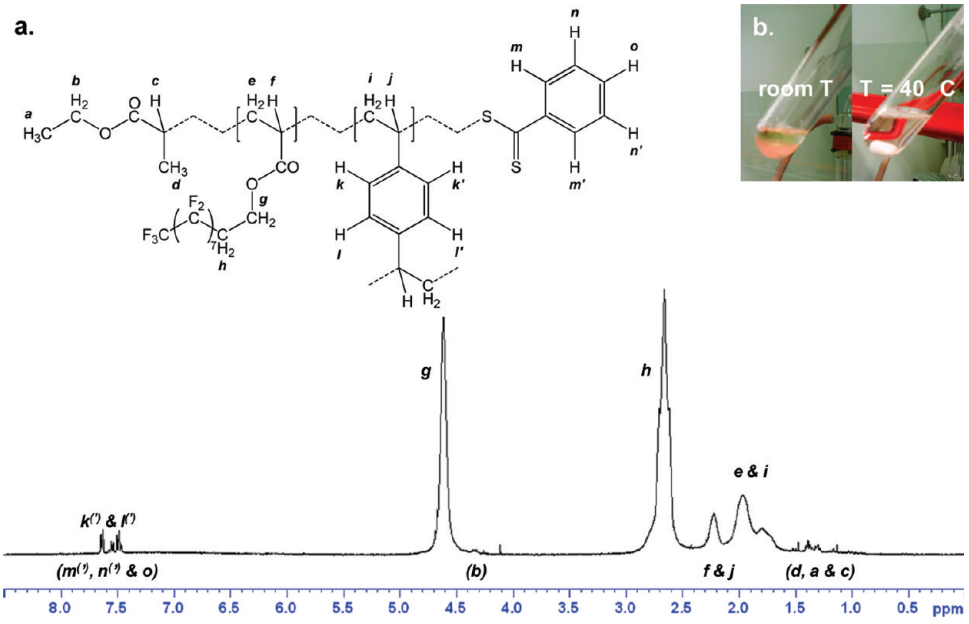

Figure 4. (a) ^{1}H NMR spectrum of poly(1*H*,1*H*,2*H*,2*H*-perfluorodecyl acrylate)-based star polymers in CF_3-COOD. (b) The product was purified from residual monomers and from a fraction of residual linear precursors by successive precipitations and redissolutions in TFT, playing on temperature.

Table 2. Differential Scanning Calorimetry Experiments Results for Poly(1*H*,1*H*,2*H*,2*H*-perfluorodecyl acrylate)-Based Polymers[a]

sample type	DP of primary chains	x (%)	T_m (°C)	ΔH_m (J/g)
linear	50	0	71.1	17.7
nanogel	50	10.0	62.5	15.4
nanogel	50	15.0	59.6	13.2
nanogel	50	20.0	54.9	12.1
nanogel	50	22.0	54.4	10.0
macrogel	50	23.0	54.5	10.0
macrogel	50	25.0	53.5	9.4
macrogel	50	30.0	49.4	8.0
linear	100	0	72.4	16.8
starlike	100	3.0 cross-links per chain	70.8	8.3

[a] DP: degree of polymerization. x: initial proportion of acrylic functions belonging to cross-linker molecules. Melting temperatures (T_m) and enthalpies (ΔH_m).

at 90 °C. As soon as the melting point is reached, the product is recovered by a slide coverslip which is moved for a homogeneous spreading before allowing the sample to cool to ambient temperature.

Transmission and reflection optical microscopies were used also to observe the dewetting of fluorinated films (~25 μg/cm^2) on various substrates (glass, silicon wafers, and mica) after annealing at 90 °C and during various durations (up to 1 week).

Contact angle measurements were carried out on a Krüss DSA100 system at room temperature. A 2 μL water droplet was deposited on the sample. A charge-couple-device camera was used to capture the images of the droplets for the determination of the contact angles. Samples were prepared by deposition of solutions at 1.0 mg/mL in TFT onto clean glass (~25 μL/cm^2) and subsequent annealing at 90 °C (above the measured melting points) after solvent evaporation at ambient temperature.

Atomic force microscopy (AFM) images were recorded in air with a Nanoscope IIIa microscope operating in tapping mode. The probes were commercially available silicon tips with a spring constant of 42 N/m, a resonance frequency of 285 kHz, and a typical radius of curvature in the 8−10 nm range. The roughness of the surfaces was quantified by determination of the root-mean-square (rms), defined as the standard deviation of the Z values within the box cursor:

$$\mathrm{rms} = \sqrt{\frac{\sum Zi}{n}}$$

where Zi is the current Z value and n the number of points.

Freshly cleaved highly ordered pyrolytic graphite (HOPG) was used as sample substrate materials. For the observation of isolated objects and the characterization of crystallization tendency, sample solutions in TFT at concentrations ranging from 10 μg/mL to 1.0 mg/mL were deposited on the substrate (20 μL) and immediately spin-coated (duration: 60 s; rate: 1500−4500 rpm). AFM was also used to put in evidence the effect of annealing at 90 °C on films prepared by deposit on HOPG (~25 μg/cm^2).

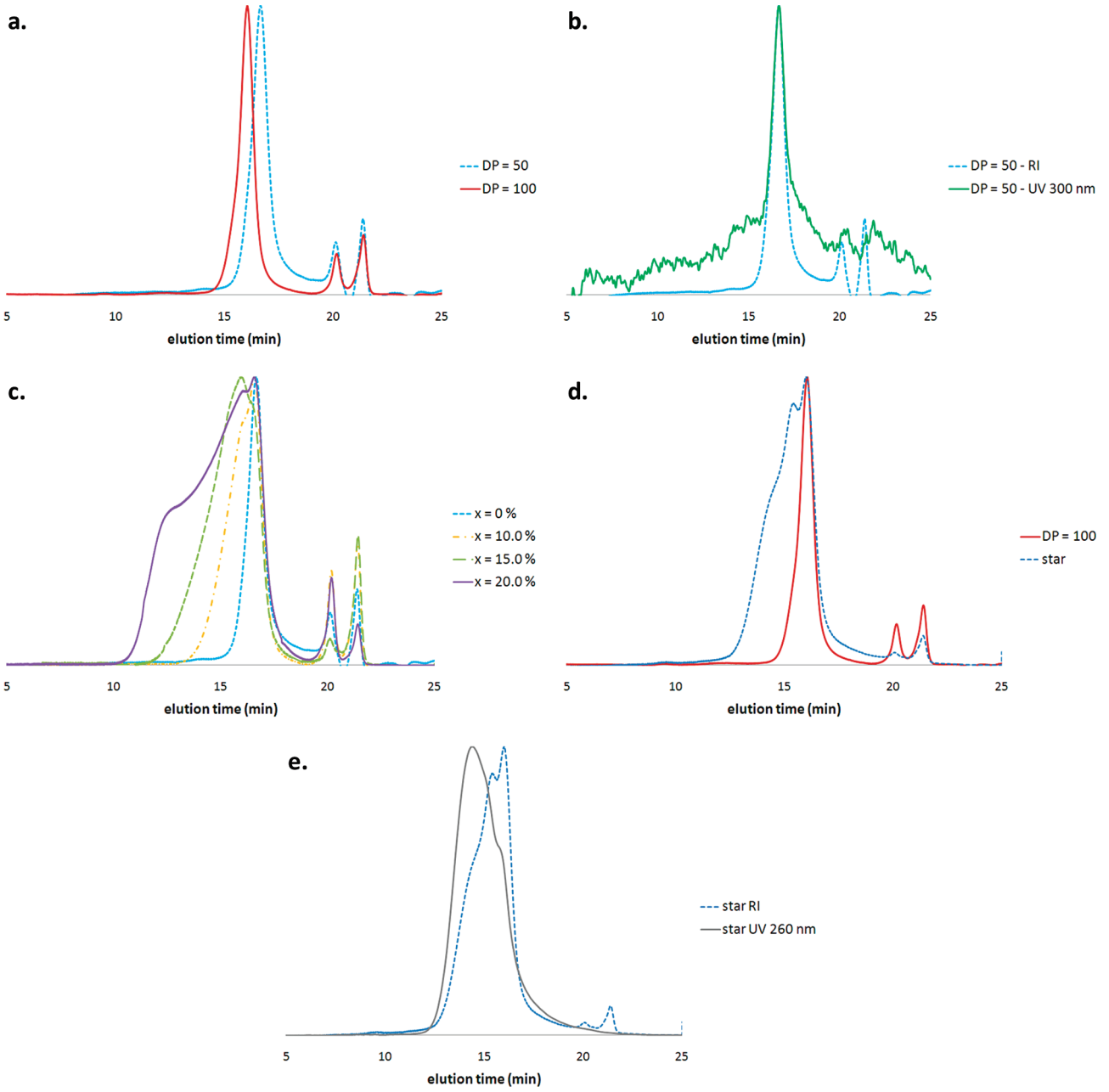

Figure 5. Steric exclusion chromatograms of poly(1*H*,1*H*,2*H*,2*H*-perfluorodecyl acrylate)-based polymers in hexafluoroisopropanol. (a) Effect of the targeted degree of polymerization (DP) for linear samples (DP = 50 and DP = 100). (b) Evidence of the presence of dithioester chain end functionalities for a linear polymer (DP = 50): overlap between RI chromatogram and UV chromatogram at 300 nm. (c) Effect of the initial proportion of acrylic functions belonging to cross-linker molecules (x). Total initial concentration of acrylic functions: C_0 = 0.500 mol/kg. Initial concentration of chain transfer agent: $[CTA]_0 = 1.00 \times 10^{-2}$ mol/kg. (d) RI chromatograms: starlike polymers vs linear precursors. (e) Evidence of the presence of divinylbenzene cross-links for the starlike polymer: comparison between RI chromatogram and UV chromatogram at 260 nm.

Relative molar masses of linear poly(PFDA) were determined by means of size exclusion chromatography (SEC) in 1,1,1,3,3,3-hexafluoro-2-propanol (HFIP) + 0.05 wt % of potassium trifluoroacetate, at a flow rate of 1.0 mL/min using a Varian ProStar 210 pump. The columns set consisted in two Polymer Laboratories PL 1114-6900HFIP columns (300 × 7.5 mm; bead sizes: 9 μm) at a temperature of 40 °C. Poly(methyl methacrylate) standards were used for the calibration. Samples were prepared at a concentration of 3.5 mg/mL. Solutions were filtrated prior to injection using PTFE 0.2 μm filters. The volume of injection was 20 μL. A Varian Prostar 355 RI detector and a Varian 2550 UV detector at 300 nm (for dithiobenzoate chain ends) or at 260 nm (for aromatic cycles) connected in series were used.

Results and Discussion

Synthesis of Fluoro-Based Linear and Branched Polyacrylates. The RAFT agent, namely ethyl 2-[(phenylcarbonothioyl)sulfanyl]propanoate, used in this work has already been reported to efficiently control the polymerization of PFDA.[19] Nanogels based on PFDA were prepared by CRCC in solution in α,α,α-trifluorotoluene (TFT) using 1,4-butanediol diacrylate (BDDA) as cross-linker and AIBN as radical source. In all the polymerizations carried out, the PFDA conversions were higher than 94% as determined by ^{1}H NMR spectroscopy. A typical spectrum of a nanogel with all peaks assignment is given in Figure 3. For the synthesis of nanogels, the efficiency of BDDA as a cross-linker was investigated trough the increase of

the initial ratio $x = 2[BDDA]_0/(2[BDDA]_0 + [PFDA]_0)$ of double bonds belonging to BDDA, for fixed initial concentrations in CTA, initiator, and double bonds C_0. With these parameters, the length of the constitutive chains at complete conversion is imposed by the relation $DP_{ch} = C_0/([CTA]_0 + 2f[AIBN]_0) \approx C_0/[CTA]_0$, with f being the efficiency of initiator. For $C_0 = 0.500$ mol/kg and $[CTA]_0 = 1.00 \times 10^{-2}$ mol/kg, a sharp transition between soluble products and macroscopic gels at complete conversion is observed in the interval $22.0\% < x < 23.0\%$ (inset in Figure 3).

In the case of starlike polymers, 23 equiv of DVB compared to arm precursors was used. The average experimental DP of precursors was 96, as determined by ^{1}H NMR spectroscopy. Interestingly, stars were insoluble in TFT at ambient temperature, on the contrary to linear precursors, whereas they were soluble over 40 °C (inset in Figure 4). It was thus possible to easily purify the product from residual monomers and from a fraction of residual linear precursors by performing successive cycles of precipitation, removal of supernatant, and redissolution in pure TFT. In the purified product, we determined by ^{1}H NMR spectroscopy that the stars comprised an average of 3.0 converted DVB units per arm, through the comparison of integrals corresponding to protons g and h with those of protons k and l (Figure 4; calculations detailed in Experimental Section).

Characterization of Fluoro-Based Linear and Branched Polyacrylates. All the soluble poly(PFDA) samples were analyzed by SEC in hexafluoroisopropanol. Apparent molar masses and molar mass distributions relative to poly(methyl methacrylate) standards are summarized in Table 1.

The obtained SEC results supported an efficient control of the polymerization, as shown by the unimodal and symmetrical shape of the chromatograms and by the increase of molar mass as a function of the monomer to CTA ratio observed for linear samples (Figure 5a). The efficiency of the control is additionally supported by the overlap of RI signals with UV signals at 300 nm, the wavelength characterizing the presence of remaining dithioester chain end functionalities (Figure 5b). The important noise observed for the UV signal can be explained by the very low relative concentration of dithioester chain end functionalities due to the high molar mass of the monomer used in the present study. The length of the primary chains of nanogels is expected to be controlled as well, as proved by several experimental studies of CRCC in which cross-links were cleaved to access the molar mass distribution of these constitutive chains.[14,20−22] In the case of constitutive chains with a targeted DP equal to 50, the effect of the initial proportion of acrylic functions belonging to cross-linker molecules x is in agreement with the trends observed in aforementioned studies: an increase of x results in higher molar masses and broader molar mass distributions due to an increase of intermolecular cross-linking (Figure 5c).

As for the cross-link density, very high [BDDA]/[CTA] ratios were used (up to 11 in the case $[CTA] = C_0/50$ and $x = 22\%$) while keeping the products perfectly soluble at complete conversions. This is indicative of an important contribution of intramolecular cross-linking, which results in the formation of network structures. As described in previous reports indeed, the control of the polymerization enables to tune finely the respective proportions of inter- and intramolecular cross-linking by playing in particular on the concentration of polymerizable functions C_0 while the formation of a macroscopic gel is prevented.[12] In the present study, the concentration C_0 was kept quite low on purpose so as to form densely cross-linked nanogels.

In the case of starlike polymers, the comparison of the RI chromatogram with the one corresponding to linear precursors revealed an important increase of the molar mass, confirming the efficiency of the convergent cross-linking step by DVB (Figure 5d). However, a significant amount of residual linear precursors is also observed; the average number of cross-links per chain calculated previously from the ^{1}H NMR spectrum is therefore underestimated. The formation of DVB cross-linked cores is also confirmed by the comparison of the RI signal with the UV signal at 260 nm, the wavelength characterizing the presence of DVB units: the UV signal is indeed more intense for the higher molar masses (Figure 5e).

Crystallization of Fluoro-Based Linear and Branched Polyacrylates. The high tendency of poly(PFDA) and similar fluorinated comb polymers to crystallize in a smectic B phase has been yet reported.[23,24] We investigated here the crystalline properties of both the nanogels and the "arm-first" stars based on poly(PFDA) as a function of their cross-link density. Indeed, the cross-links statistically introduced along the chains in the case of nanogels or the convergent cross-linking of linear precursors in the case of "arm-first" starlike polymers should inhibit the crystallization phenomenon. Analysis by polarized optical microscopy on glass revealed an apparent disappearance of birefringence and thus of crystallinity as the cross-link density of nanogels increased (insets in Figure 6a). A similar trend was also observed for the DVB cross-linked polymeric stars (insets in Figure 6b). These observations are in good agreement with the data collected by DSC which showed that an increase of the cross-link density for the nanogels series resulted in a decrease of the melting point and of the melting enthalpy relative to the transition from a smectic B to an isotropic phase (Table 2 and Figure 6a). These results indicate a dramatic loss of organization of the pendant fluorinated chains due to limitation of accessible conformations induced by cross-links. The convergent cross-linking of linear precursors to prepare starlike polymers goes also with a significant decrease of the melting enthalpy (Table 2 and Figure 6b) ascribable to the formation of densely cross-linked cores, which hampers the crystallization of chains. The transition observed by DSC can be explained by the local crystallization of arms and/or by the crystallization of residual linears.

A deeper insight into the phenomenon was gained by tapping mode AFM of the fluoro-based polymers deposited on a HOPG substrate. AFM images observed from fluorinated nanogels and star polymers are reported for the first time. In the case of the linear sample, we observed a 0.6 nm thick monolayer composed of regular stripes of a few hundred nanometers in length, indicating the formation of structured crystalline domains (Figure 7a). We determined that the average distance between two consecutive stripes was around 6 nm (scheme in Figure 7). This value is higher than that measured by other groups by means of X-ray diffraction, which was around 4 nm.[23,24] This difference may be due to the fact that, in the present study, crystallization proceeds by an epitaxial growth governed by the strong affinity between the pendant fluorinated chains and the HOPG substrate. For the nanogels series, the increase of the cross-link density results in a progressive inhibition of crystallization with in particular an organization over shorter distances and heterogeneities indicative of domains locally cross-linked (Figure 7b). For high cross-link densities, no crystallization is observed any longer, whereas globular objects having an average diameter of 20 nm can be distinguished (Figure 8c). These observations are consistent with the aforementioned expected evolution of the products topology through the increase of the cross-link

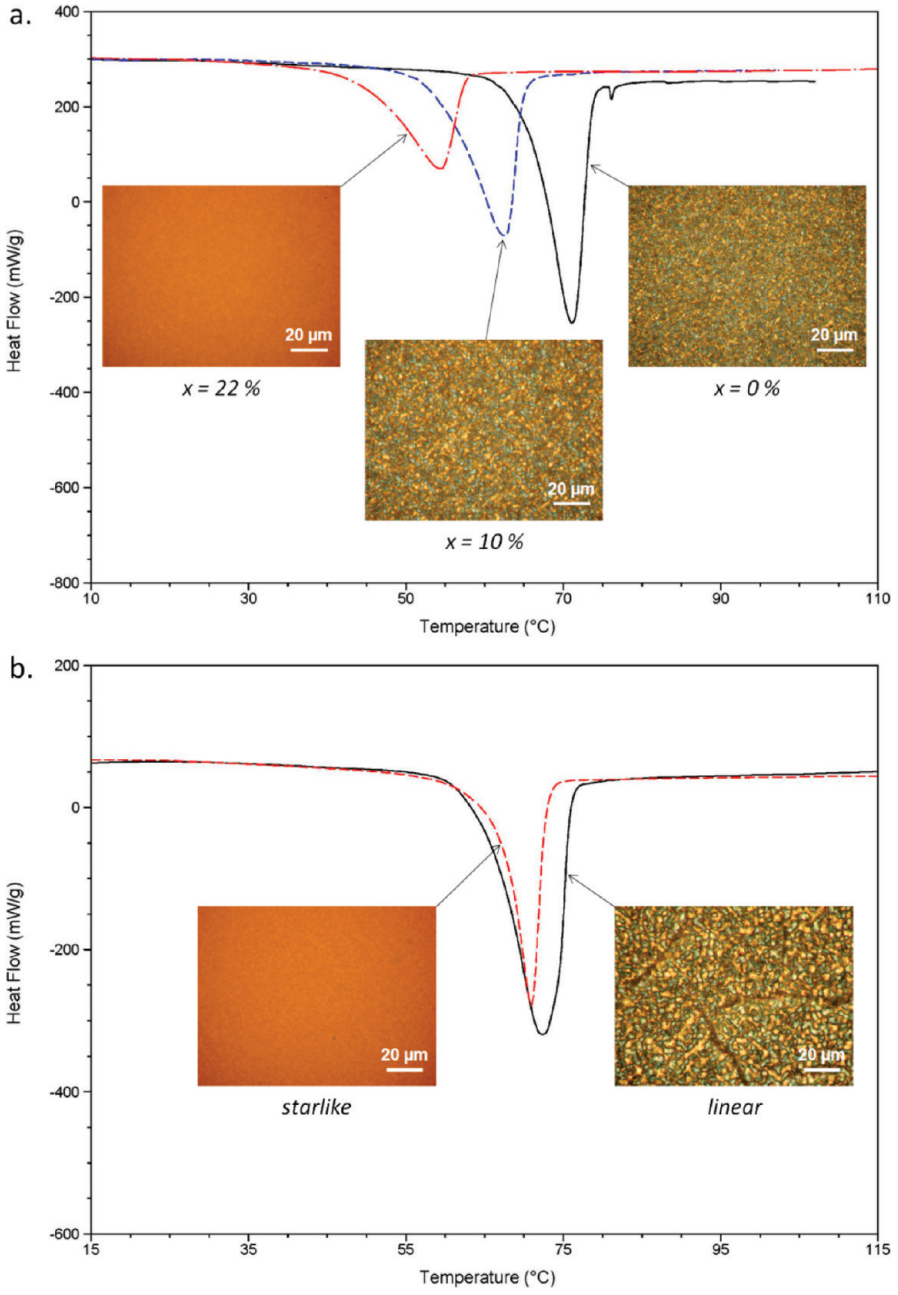

Figure 6. Differential scanning calorimetry curves for poly(1*H*,1*H*,2*H*,2*H*-perfluorodecyl acrylate)-based polymers and corresponding polarized optical microscopy images under the melting point. $C_0 = 0.500$ mol/kg, $[CTA]_0 = 1.00 \times 10^{-2}$ mol/kg. (a) Nanogels series: DP of primary chains = 50; influence of the initial proportion of acrylic functions belonging to cross-linker molecules (x): —, $x = 0\%$ (linear); - - -, $x = 10.0\%$; - · -, $x = 22.0\%$. (b) Starlike polymers: DP of arms = 100: —, linear precursor; - - -, starlike polymers.

density: linear, then branched, and finally highly branched with a 3D network structure.

In the case of starlike polymers, the disappearance of crystallization over long distances is also observed (Figure 7d). AFM reveals the formation of rather dense globular objects surrounded by softer coronas. This observation is consistent with the formation of rigid poly(DVB) cores from which emanate fluorinated hairy poly(PFDA) chains. This is also supported by the presence of visible stripes in the coronas, with a typical distance between two consecutive stripes around 4−6 nm, values aforementioned in the case of the crystallization of the corresponding homopoly(PFDA). It is highly likely that the local crystalline domains correspond to the arms of stars and residual linear precursors and account for the transition detected by DSC, whereas no residual anisotropy was observed by polarized optical microscopy (Table 2 and Figure 6b).

Thermal Stability of Fluorinated Films. These discrepancies in terms of nanometric organizations between branched and linear polymers are expected to modify notably intermolecular interactions, thus resulting in different macroscopic properties. In this respect, we investigated the wettability of fluorinated films prepared from these samples and their evolution upon annealing. Very similar contact angles were measured for both the nanogels and for the linear reference, the corresponding films being highly hydrophobic with contact angle values comprised typically between 115° and 120°. However, the films responded differently to an annealing at 90 °C (temperature over the melting points of the samples): an important decrease of the contact angle

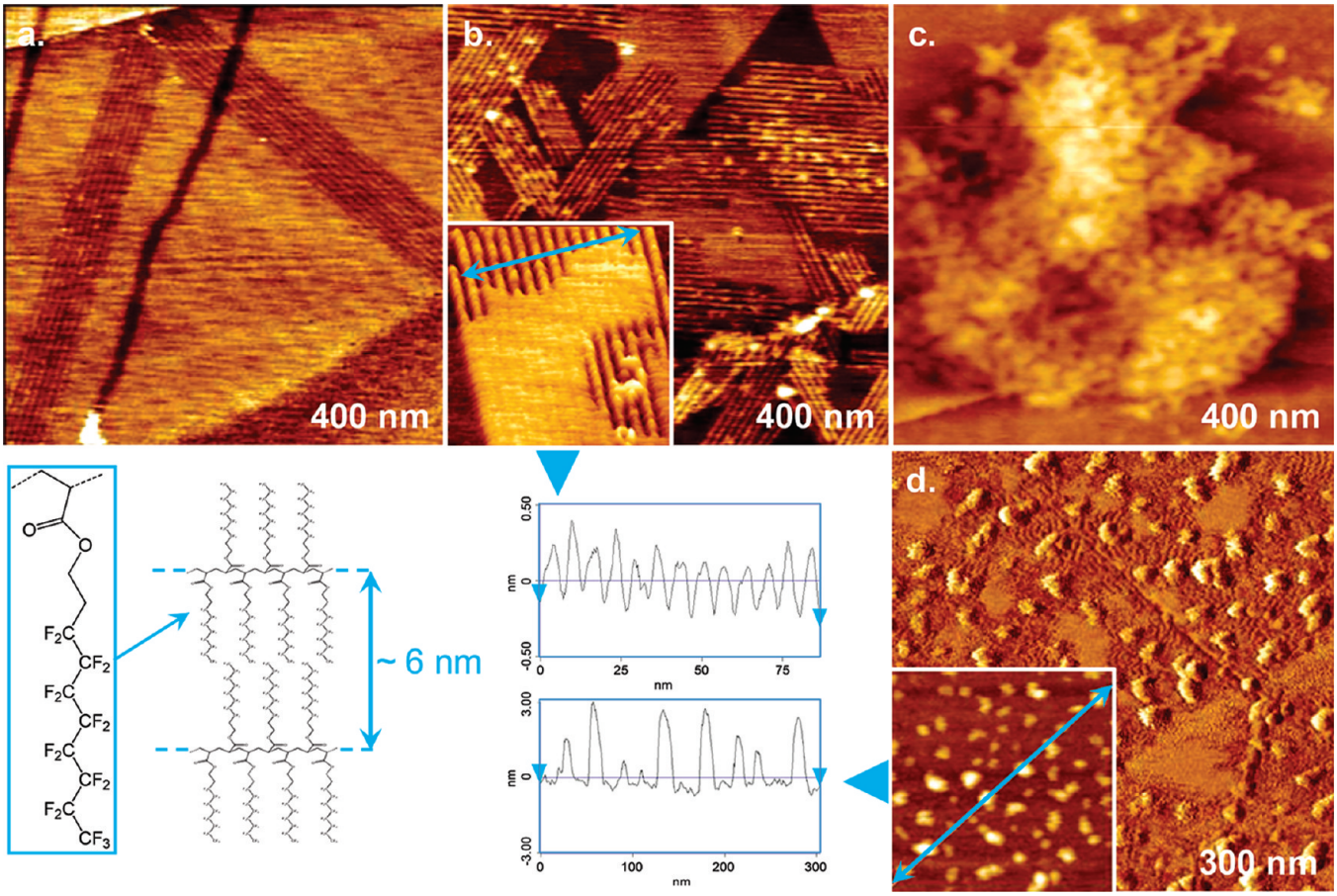

Figure 7. Atomic force microscopy (AFM) images and profiles results for poly(1*H*,1*H*,2*H*,2*H*-perfluorodecyl acrylate)-based polymers and scheme showing the crystallization resulting from fluorinated pendant chains. DP: degree of polymerization. *x*: initial proportion of acrylic functions belonging to cross-linker molecules. Nanogels series (DP of primary chains = 50, $[CTA]_0 = 1.00 \times 10^{-2}$ mol/kg). AFM topography images: (a) $x = 0\%$ (linear); (b) $x = 10.0\%$ (inset for profile); (c) $x = 22.0\%$. Starlike polymers (DP of arms = 100): (d) phase image (inset: topography image for profile).

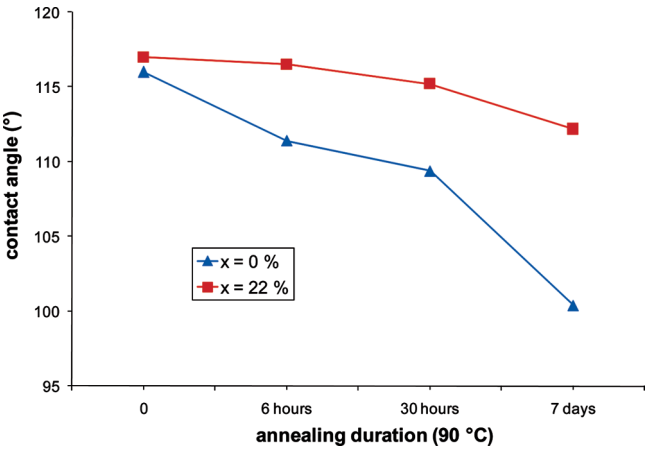

Figure 8. Contact angles measured for water droplets (2 μL) deposited on fluorinated films on glass prepared from nanogels and from corresponding linears. Initial films and films after annealing at 90 °C. *x*: initial proportion of acrylic functions belonging to cross-linker molecules.

was observed for the film prepared from linear polymers while the hydrophobicity was almost preserved for the one prepared from nanogels (Figure 8). These results are indicative of a better covering stability upon annealing in the case of nanogels as compared to linear polymers.

Complementary studies were carried out on these films by optical microscopy in order to determine the origin of this discrepancy. For a same initial thickness, totally different behaviors were observed on various substrates (glass, silicon wafer, mica) between films resulting either from linear polymers or from parent branched architectures (nanogels or stars). The film aspect is almost not modified by annealing in the case of branched architectures, whereas a dramatic dewetting of the polymeric film on the substrate is observed in the case of linear samples (Figure 9).

The dewetting of fluorinated polymers over hydrophilic surfaces is ascribable to the low surface energy brought into play. The retracting of polymer so as to minimize the interface with the substrate is therefore energetically favored. The introduction of cross-links enables a strong inhibition of this phenomenon, through the limitation of the chains reptation. In the case of linear samples, the chains can rearange separately over the melting temperature so as to minimize the interaction with the substrate. This is no longer the case for branched polymers in which covalent interactions exist between the chains. Therefore, the higher the cross-link density of the film is, the less the chains can rearrange, which results in the prevention of the substrate dewetting. This strategy is classically implemented by the curing of films subsequently to their coating. In this work, a similar reinforcement of films results from cross-links formed ab initio and built-in in soluble branched architectures.

A deeper insight of this behavior was obtained by AFM on films prepared on HOPG. Despite the surface being initially rougher in the case of films prepared from branched architectures than for those prepared from linear polymers, an

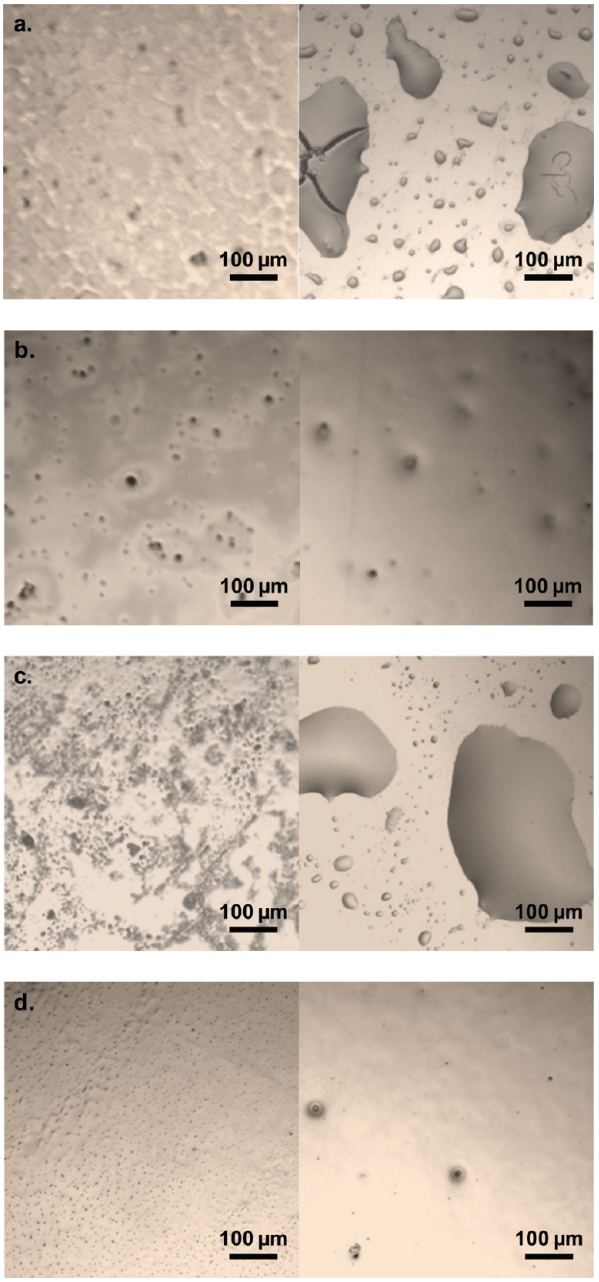

Figure 9. Aspects of films on silicon wafers prepared from poly(1*H*,1*H*,2*H*,2*H*-perfluorodecyl acrylate)-based branched architectures and corresponding linears before and after annealing at 90 °C for 5 days (left and right images, respectively), observed by reflection optical microscopy: (a) linear DP = 50; (b) nanogel DP_{ch} = 50 and x = 22.0%; (c) linear DP = 100; (d) starlike DP_{ch} = 100. DP: degree of polymerization. x: initial proportion of acrylic functions belonging to cross-linker molecules.

annealing resulted in a rapid and dramatic dewetting of the polymer on the substrate in the case of linears, whereas the initial roughness of the film was almost preserved in the case of branched architectures (Figure 10).

It is worth noting that the dewetting did not reach a macroscopic scale in this case because HOPG is more hydrophobic than the aforementioned substrates, such as glass or silicon wafers. However, the formation of numerous polymeric plots surrounded by areas where the substrate is discovered caused here also a global decrease of the hydrophobicity of the surface, probed by lower contact angle values for deposited water droplets of 2 μL.

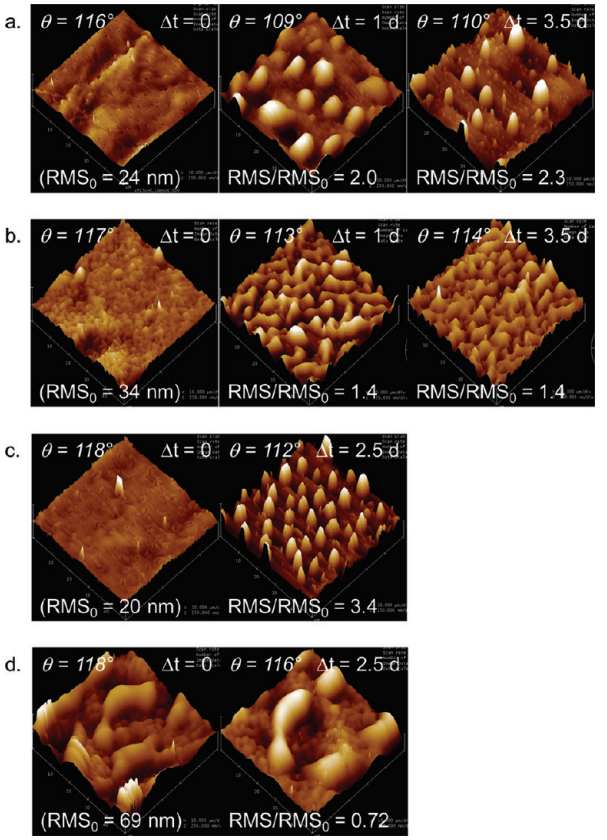

Figure 10. Atomic force microscopy 3D-topography images (50 μm × 50 μm) of films prepared from from poly(1*H*,1*H*,2*H*,2*H*-perfluorodecyl acrylate)-based branched architectures and corresponding linears before and after annealing at 90 °C. RMS: root-mean-square; θ: contact angle for deposited water droplets of 2 μL; Δt: duration of annealing. (a) Linear DP = 50; (b) nanogel DP_{ch} = 50 and x = 22.0%; (c) linear DP = 100; (d) starlike DP_{ch} = 100. DP: degree of polymerization. x: initial proportion of acrylic functions belonging to cross-linker molecules.

Conclusions

Controlled radical cross-linking copolymerization was applied for the first time to the synthesis of two types of fluorinated soluble branched architectures based on 1*H*,1*H*,2*H*,2*H*-perfluorodecyl acrylate (PFDA), namely nanogels and starlike polymers. For this purpose, it was resorted to a RAFT process using a dithioester as a chain transfer agent. The initial parameters were screened in order to control the final structure in terms of cross-link density, chain length, and composition. Increasing cross-link density resulted in the decrease of crystallinity. For densely cross-linked nanogels, the crystallization was totally inhibited. These different cross-link densities and resulting topologies directly impacted the macroscopic properties of films prepared from these polymeric materials. An enhanced thermal stability of the film structure was obtained for branched macromolecules, despite their melting point being lower than that of comparable linear polymers. Consequently, the hydrophobicity of the surface was preserved with branched materials after annealing, while films prepared from linear polymers submitted to the same thermic treatment became significantly less hydrophobic.

The ab initio introduction of cross-links, through the implementation of soluble branched architectures, is therefore an efficient means to prevent the dewetting of films on substrates from the microscopic to the macroscopic scale. It also offers an easy alternative route to reinforce coatings for industrial purposes, with in particular no need for a postpolymerization curing.

Acknowledgment. J. Rodriguez-Hernandez is thankful to the Agence Nationale pour la Recherche (ANR) for financial support of the "ADPOLYSURF" project (JC-0718-5698). D. Taton is also grateful to the ANR for financial support of the "RAFT in Gels" project (JCJC06_154178).

References and Notes

(1) Plunkett, R. J. US Patent 1941/2,230,654.
(2) *Modern Fluoropolymers*; Scheirs, J., Ed.; Wiley: New York, 1997.
(3) *Fluoropolymers: Synthesis and Properties*; Hougham, G., Johns, K., Cassidy, P. E., Davidson, T., Eds.; Plenum Press: New York, 1999.
(4) *Well-Architectured Fluoropolymers: Synthesis, Properties and Applications*; Ameduri, B., Boutevin, B., Eds.; Elsevier: Amsterdam, 2004.
(5) *Fluorinated Coatings and Finishes Handbook*; McKeen, L. W., Ed.; William Andrew Publishing: Norwich, 2006.
(6) Hansen, N. M. L.; Jankova, K.; Hvilsted, S. *Eur. Polym. J.* **2007**, *43*, 255–293.
(7) Hirao, A.; Sugiyama, K.; Yokoyama, H. *Prog. Polym. Sci.* **2007**, *32*, 1393–1438.
(8) Destarac, M.; Bavouzet, B.; Taton, D. Int. Pat. WO 2004/014535.
(9) Taton, D. In *Macromolecular Engineering*; Matyjaszewski, K., Leibler, L., Gnanou, Y., Eds.; Wiley-VCH: Weinheim, 2007; Vol. *2*, p 1007.
(10) Gao, H.; Matyjaszewski, K. *Prog. Polym. Sci.* **2009**, *34*, 317–350.
(11) Gao, H.; Miasnikova, A.; Matyjaszewski, K. *Macromolecules* **2008**, *41*, 7843–7849.
(12) Poly, J.; Wilson, D. J.; Destarac, M.; Taton, D. *J. Polym. Sci., Part A: Polym. Chem.* **2009**, *47*, 5313–5327.
(13) Taton, D.; Baussard, J.-F.; Dupayage, L.; Poly, J.; Gnanou, Y.; Ponsinet, V.; Destarac, M.; Mignaud, C.; Pitois, C. *Chem. Commun.* **2006**, *18*, 1953–1955.
(14) Poly, J.; Wilson, D. J.; Destarac, M.; Taton, D. *Macromol. Rapid Commun.* **2008**, *29*, 1965–1972.
(15) IUPAC *Pure Appl. Chem.* **2007**, *79*, 1801−1829.
(16) Barner-Kowollik, C.; Davis, T. P.; Stenzel, M. H. *Aust. J. Chem.* **2006**, *59*, 719–727.
(17) Rizzardo, E.; Moad, G.; Thang, S. H. In *Handbook of RAFT Polymerization*; Barner-Kowollik, C., Ed.; Wiley-VCH: Weinheim, 2008; p 189.
(18) Severac, R.; Lacroix-Desmazes, P.; Boutevin, B. *Polym. Int.* **2002**, *51*, 1117–1122.
(19) Rixens, B.; Severac, R.; Boutevin, B.; Lacroix-Desmazes, P. *Polymer* **2005**, *46*, 3579–3587.
(20) Li, Y.; Armes, S. P. *Macromolecules* **2005**, *38*, 8155–8162.
(21) Wang, A. R.; Zhu, S. *J. Polym. Sci., Part A: Polym. Chem.* **2005**, *43*, 5710–5714.
(22) Oh, J. K.; Tang, C.; Gao, H.; Tsarevsky, N. V.; Matyjaszewski, K. *J. Am. Chem. Soc.* **2006**, *128*, 5578–5584.
(23) Fujimori, A.; Masuya, R.; Masuko, T.; Ito, E.; Hara, M.; Kanai, K.; Ouchi, Y.; Seki, K.; Nakahara, H. *Polym. Adv. Technol.* **2006**, *17*, 653–663.
(24) De Crevoisier, G.; Fabre, P.; Leibler, L.; Tenc-Girault, S.; Corpart, J. M. *Macromolecules* **2002**, *35*, 3880–3888.